Zero- and Two-Dimensional Organization of Tetrahedral Cadmium Chalcogenide Clusters with Bifunctional Covalent Linkers

Nanfeng Zheng,[†] Xianhui Bu,[‡] Jason Lauda,[†] and Pingyun Feng*,[†]

Department of Chemistry, University of California, Riverside, California 92521, and Department of Chemistry and Biochemistry, California State University, 1250 Bellflower Boulevard, Long Beach, California 90840

Received March 8, 2006. Revised Manuscript Received June 16, 2006

Few examples are known in which chalcogenide clusters are assembled with organic ligands into crystallographically ordered covalent superlattices even though molecular crystals of such clusters have been known for decades. Here by using bifunctional organic ligands as the organizing force, semiconducting tetrahedral chalcogenide clusters, $Cd_{32}S_{14}(SPh)_{36}$, have been assembled into two-dimensional layers. In addition, a dimeric unit consisting of two core−shell-like $C_{17}Se_4(SPh)_{26}$ clusters bridged by two organic ligands has also been synthesized. In these inorganic−organic hybrid assemblies, chalcogenide clusters and bifunctional organic ligands are joined together through metal−ligand coordination bonds. A key structural feature is the presence of two organic bridging ligands between the same two clusters (the double-bridging mode). This work demonstrates the feasibility of creating organized nanocluster−ligand superstructures through synthetic design of molecular clusters or bridging ligands.

Introduction

In the area of nanostructured materials, chalcogenide clusters such as $Cd_{17}S_4(SPh)_{28}^{2-}$ and $Cd_{32}Se_{14}(SePh)_{36}(PPh_3)_4$ occupy a position at the extreme lower limit of the size spectrum of nanoparticles of which size-dependent properties have been recognized as key to future technological advancement.[1,2] Unlike colloidal nanoparticles, chalcogenide nanoclusters have unique advantages resulting from their precisely defined size and composition.[3−6] In addition to potential applications in nanotechnology, they could serve as model systems and provide synthetic and structural insights into the formation, structure, and properties of larger colloidal nanoparticles and their superlattices that usually have less well-defined structures.

Nanocluster superlattices that are periodic arrays of nanoclusters represent a new class of materials that are different from either individual nanoclusters or condensed solids. The collective properties of nanocrystal superlattices are dependent on individual clusters, cross-linking ligands if present, and their spatial organization. For example, the activation energy for electron transfer between nanoparticles has been found to depend on the cluster−cluster distance in the case of noncovalent linkage, and in the case of covalent linkage, the transport properties of the spacer play an important role.[7]

In addition to unique electronic and optical properties, nanocluster superlattices may also have potential uses as functional nanoporous materials because of their open architecture. Unlike traditional oxide microporous materials that are usually insulating, semiconducting nanocluster superlattices may have useful optical or electrooptic properties. Such integration between uniform porosity and semiconductivity in nanocluster superlattices can lead to new applications in areas such as shape- or size-selective photocatalysis and electrochemical solar cells.[8]

Currently, there are two common types of chalcogenide nanocluster superlattices. In the first type, chalcogenide nanoclusters such as $Cd_{32}S_{14}(SPh)_{36}(DMF)_4$ (DMF = *N*,*N*-dimethylformamide) crystallize through noncovalent interactions to form molecular crystals.[9−11] In such molecular crystals, clusters tend to form closed packed structures, and few routes are available to allow the assembly of these clusters into different spatial patterns. In the second type, nanoclusters (e.g., $In_{10}S_{18}^{6-}$, $In_{16}Cd_4S_{33}^{10-}$, and $Cd_{17}S_4(SCH_2CH_2OH)_{26}$) are joined together through corner-sharing chalcogens (e.g., S^{2-}, SPh^-, and S_3^{2-}) to form rigid covalent

* To whom correspondence should be addressed. E-mail: pingyun.feng@ucr.edu.
[†] University of California.
[‡] California State University.

(1) Lee, G. S. H.; Craig, D. C.; Ma, I.; Scudder, M. L.; Bailey, T. D.; Dance, I. G. *J. Am. Chem. Soc.* **1988**, *110*, 4863−4864.
(2) Soloviev, V. N.; Eichhofer, A.; Fenske, D.; Banin, U. *J. Am. Chem. Soc.* **2001**, *123*, 2354−2364.
(3) Dance, I. G.; Fisher, K. *Prog. Inorg. Chem.* **1994**, *41*, 637−803.
(4) Krebs, B.; Henkel, G. *Angew. Chem., Int. Ed.* **1991**, *30*, 769−788.
(5) (a) Feng, P.; Bu, X.; Zheng, N. *Acc. Chem. Res.* **2005**, *38*, 293−303. (b) Bu, X.; Zheng, N.; Feng, P. *Chem.—Eur. J.* **2004**, *10*, 3356−3362.
(6) Corrigan, J. F.; Degroot, M. W. In *The Chemistry of Nanomaterials: Synthesis, Properties and Applications*; Rao, C. N. R., Müller, A., Cheetham, A. K., Eds.; Wiley: Weinheim, 2004; Vol. 2, pp 418−451.
(7) Torma, V.; Vidoni, O.; Simon, U.; Schmid, G. *Eur. J. Inorg. Chem.* **2003**, 1121−1127.
(8) Zheng, N.; Bu, X.; Vu, H.; Feng, P. *Angew. Chem., Int. Ed.* **2005**, *44*, 5299−5303.
(9) Herron, N.; Calabrese, J. C.; Farneth, W. E.; Wang, Y. *Science* **1993**, *259*, 1426−1428.
(10) Vossmeyer, T.; Reck, G.; Schulz, B.; Katsikas, L.; Weller, H. *J. Am. Chem. Soc.* **1995**, *117*, 12881−12882.
(11) Behrens, S.; Bettenhausen, M.; Deveson, A. C.; Eichhoefer, A.; Fenske, D.; Lohde, A.; Woggon, U. *Angew. Chem., Int. Ed.* **1996**, *35*, 2215−2218.

10.1021/cm060557z CCC: $33.50
Published on Web 08/05/2006

Table 1. Summary of Crystallographic Data for Co-Assemblies Synthesized in This Study

name[a]	COV-5 CdS-TMDPy	COV-7 CdS-BPEA	COV-8 CdSeS-TMDPy
cluster type	C2,1 CdS	C2,1 CdS	C1 CdSeS
cluster composition[b]	$Cd_{32}S_{14}(SPh)_{36}L_4$	$Cd_{32}S_{14}(SPh)_{36}L_4$	$Cd_{17}Se_4(SPh)_{26}L_2$
space group	$P2_1/n$	$P2_1/c$	$P2_1/c$
a (Å)	22.0477(2)	22.6957(4)	32.028(6)
b (Å)	61.0454(7)	21.8142(4)	27.889(6)
c (Å)	22.2861(3)	57.6612(10)	42.198(9)
β (deg)	94.011(1)	93.245(1)	99.636(5)
$R(F)$	5.69	5.43	7.68

[a] TMDPy = 4,4′-trimethylenedipyridine, $C_{13}H_{14}N_2$; BPEA = 1,2-bis(4-pyridyl)ethane, $C_{12}H_{12}N_2$. [b] L = pyridyl at the tetrahedral corner. The number of ligand molecules per formula unit is half of the number of pyridyl groups.

superlattices.[12−18] One limitation with this approach comes from the inflexible M−X−M angle (M = metal ions and X = chalcogens) that places a significant constraint on the number of topological types that can be achieved.

In this research, to overcome above limitations and to expand compositional and topological diversity of nanocluster superlattices, we employ bifunctional organic ligands as the organizing force to stabilize and assemble semiconducting nanoclusters into crystallographically ordered superlattices. The structural diversity of organic ligands, together with the size, composition, and topological tunability of chalcogenide nanoclusters, opens up a rich opportunity for the creation of a variety of unprecedented nanocluster superlattices.

Prior to our work, few examples of the covalent co-assembly between chalcogenide nanoclusters and organic ligands exist. However, very recently, a series of one-dimensional covalent superlattices were created from different cadmium chalcogenide clusters and organic ligands.[19,20] In this work, among various bifunctional molecular ligands, bipyridines have been selected to organize chalcogenide nanoclusters into unique dimeric or two-dimensional superstructures. In these inorganic−organic hybrid assemblies, nanoclusters and bifunctional organic ligands are joined together through metal−ligand coordination bonds. It is further demonstrated here that organic ligands of different length and rigidity can be used for co-assembly between tetrahedral clusters and organic ligands, making it possible to create organized nanocluster−ligand superstructures through synthetic design of either nanoclusters and bridging ligands, in addition to various patterns of joining them together.

Experimental Section

Synthesis. All materials discussed in this work were synthesized under solvothermal conditions in the temperature range between 85 and 150 °C. The solvents were mainly acetonitrile, water, or their mixtures. $Cd(SPh)_2$ and $[N(CH_3)_4]_2[Cd_4(SPh)_{10}]$, the sources for Cd^{2+} and SPh^-, were synthesized by the literature method.[21,22]

COV-5 CdS-TMDPy. A total of 0.168 g of $(NMe_4)_2[Cd_4(SPh)_{10}]$, 85 mg of 4,4′-trimethylenedipyridine, 0.464 g of a 10% $Na_2S_2O_3{\cdot}5H_2O$ aqueous solution, and 10.119 g of water were mixed in a 23-mL Teflon lined stainless steel autoclave and stirred for ∼20 min. The vessel was sealed and heated at 150 °C for 3 days. After cooling to room temperature, the filtered solid product was washed with water and ethanol to give pure COV-5 CdS-TMDPy crystals.

COV-7 CdS-BPEA. A total of 1.690 g of tetraphenylphosponium bromide (PPh_4Br), 1.940 g of thiourea, and 7.652 g of $Cd(SPh)_2$ were mixed together with 100.093 g of acetonitrile and 9.141 g of water. After stirring for ∼30 min, the mixture became a clear solution. To a 25-mL thick-walled glass vial were added 2.990 g of this clear solution, 0.094 g of 1,2-bis(4-pyridyl)ethane, and 0.245 g of water. The vial was sealed and heated at 85 °C for 3 days. After cooling to room temperature, COV-7 CdS-BPEA was obtained in the form of pale yellow crystals.

COV-8 CdSeS-TMDPy. To a 23-mL Teflon lined stainless steel autoclave were added 0.214 g of 4,4′-trimethylenedipyridine, 0.017 g of Se, 0.168 g of $(NMe_4)_2[Cd_4(SPh)_{10}]$, 2.690 g of acetonitrile, and 0.420 g of water. After the mixture was stirred for ∼20 min, the vessel was sealed and heated at 110 °C for 5 days. After cooling to room temperature, a mixture of COV-8 CdSeS-TMDPy and COV-9 CdSeS $[Cd_{17}S_4(SPh)_{26}]$ was obtained.[23]

Single-Crystal Structure Analysis. Each crystal was glued to a thin glass fiber with epoxy resin and mounted on a Bruker APEX II diffractometer equipped with a fine focus, 2.0 kW sealed tube X-ray source (Mo Kα radiation, λ = 0.710 73 Å) operating at 50 kV and 30 mA. Data collections were conducted at temperatures of either 90 or 150 K. The empirical absorption correction was based on equivalent reflections, and other possible effects such as absorption by the glass fiber were simultaneously corrected. Each structure was solved by direct methods followed by successive difference Fourier methods. Computations were performed using

(12) (a) Dance, I. G.; Garbutt, R. G.; Craig, D. C.; Scudder, M. L. *Inorg. Chem.* **1987**, *26*, 4057−4064. (b) Dance, I. G.; Choy, A.; Scudder, M. L. *J. Am. Chem. Soc.* **1984**, *106*, 6285−6295.
(13) Vossmeyer, T.; Reck, G.; Katsikas, L.; Haupt, E. T. K.; Schulz, B.; Weller, H. *Science* **1995**, *267*, 1476−1479.
(14) Scott, R. W. J.; MacLachlan, M. J.; Ozin, G. A. *Curr. Opin. Solid State Mater. Sci.* **1999**, *4*, 113−121.
(15) Manos, M. J.; Iyer, R. G.; Quarez, E.; Liao, J. H.; Kanatzidis, M. G. *Angew. Chem., Int. Ed.* **2005**, *44*, 3552−3555.
(16) (a) Li, H.; Laine, A.; O'Keefe, M.; Yaghi, O. M. *Science* **1999**, *283*, 1145. (b) Li, H.; Kim, J.; Groy, T. L.; O'Keefe, M.; Yaghi, O. M. *J. Am. Chem.* Soc. **2001**, *123*, 4867−4868.
(17) (a) Cahill, C. L.; Ko, Y.; Parise, J. B. *Chem. Mater.* **1998**, *10*, 19. (b) Cahill, C. L.; Parise, J. B. *J. Chem. Soc., Dalton Trans.* **2000**, 1475−1482.
(18) (a) Zheng, N.; Bu, X.; Feng, P. *Nature* **2003**, *426*, 428−432. (b) Zheng, N.; Bu, X.; Wang, B.; Feng, P. *Science* **2002**, *298*, 2366−2369. (c) Wang, C.; Li, Y.; Bu, X.; Zheng, N. Zivkovic, O.; Yang, C.; Feng, P. *J. Am. Chem. Soc.* **2001**, *123*, 11506−11507.
(19) Zheng, N.; Bu, X.; Lu, H.; Chen, L.; Feng, P. *J. Am. Chem. Soc.* **2005**, *127*, 14990−14991.
(20) Xie, J.; Bu, X.; Zheng, N.; Feng, P. *Chem. Commun.* **2005**, 4916−4918.
(21) Dance, I. G.; Garbutt, R. G.; Craig, D. C.; Scudder, M. L. *Inorg. Chem.* **1987**, *26*, 4057−4064.
(22) Dance, I. G.; Choy, A.; Scudder, M. L. *J. Am. Chem. Soc.* **1984**, *106*, 6285−6295.
(23) COV-9 CdSeS: $Cd_{17}Se_4(SC_6H_5)_{26}$, space group *Fddd*, a = 37.977(2) Å, b = 41.050 (2) Å, c = 45.218(2) Å, V =70492(6) Å^3, Z = 16, T = 150 K, $2\theta_{max}$ = 50°, $R(F)$ = 12.13% for 661 parameters and 15 539 reflections with $I > 2\sigma(I)$. The high $R(F)$ is due to the disordered phenyl groups in the structure. COV-9 has a covalent open-framework structure consisting of two interpenetrating diamond-type lattices in each of which $[Cd_{17}Se_4(SC_6H_5)_{26}]$ (C1) clusters occupy the tetrahedral node and are connected through corner-sharing −SPh groups.

Table 2. Chemical Compositions and Charges of C*n* Clusters in the Cd^{2+}−S^{2-}−SPh− System

C*n*	idealized formula[a]	number of tetrahedral S^{2-} sites[b]	number of tricoordinated S^{2-} sites[c]	number of edge SPh^- sites[d]	number of corner SPh^- sites
C0	$Cd_8S(SPh)_{16}^{2-}$	1	0	12	4
C1	$Cd_{17}S_4(SPh)_{28}^{2-}$	4	0	24	4
C2	$Cd_{32}S_{14}(SPh)_{40}^{4-}$	10	4	36	4
C3	$Cd_{54}S_{32}(SPh)_{52}^{8-}$	20	12	48	4
C4	$Cd_{84}S_{59}(SPh)_{64}^{14-}$	35	24	60	4
C5	$Cd_{123}S_{96}(SPh)_{76}^{22-}$	56	40	72	4
C6	$Cd_{172}S_{144}(SPh)_{88}^{32-}$	84	60	84	4
C7	$Cd_{232}S_{204}(SPh)_{100}^{44-}$	120	84	96	4
C8	$Cd_{304}S_{277}(SPh)_{112}^{58-}$	165	112	108	4
C9	$Cd_{389}S_{364}(SPh)_{124}^{74-}$	220	144	120	4
C10	$Cd_{488}S_{466}(SPh)_{136}^{92-}$	286	180	132	4

[a] A C*n* cluster consists of a regular T*n* cluster at the core covered on each face with a single sheet of atoms called the T(n + 1) sheet. In addition, each corner of the T*n* cluster is covered with a MX group. The T(n + 1) sheet is defined as the bottom and the largest atomic sheet of a T(n + 1) cluster. For a C*n* cluster with the formula M_aX_b, $a = n(n + 1)(n + 2)/6 + 4(n + 1)(n + 2)/2 + 4$ and $b = (n + 1)(n + 2)(n + 3)/6 + 4(n + 2)(n + 3)/2 + 4$. Note that the number of metal sites is equal to the total number of anionic sites in the preceding member. Here, M is usually a divalent metal cation and X is a combination of divalent S^{2-} (Se^{2-}) and SR^- (or SeR^-). [b] The number of tetrahedral S^{2-} sites is the same as the number of metal sites in the T(n + 1) cluster, i.e., (n + 1)(n + 2)(n + 3)/6. [c] The tricoordinated S^{2-} sites are located on four T(n + 1) sheets. The tricoordinated S^{2-} sites in a T(n + 1) sheet is equal to the number of metal sites in a T(n − 1) sheet. The latter is equal to T(n − 1) − T(n − 2) = n(n − 1)/2. The total per cluster is 2n(n − 1). [d] The edge −SPh sites are located on four T(n + 1) sheets and are equal to 4(3n + 3).

SHELXTL, and final full-matrix refinements were against F^2. The crystallographic results are summarized in Table 1.

Results and Discussion

Tetrahedral Chalcogenide Clusters as the Inorganic Building Blocks. Chalcogenide nanoclusters that serve as structural building units here belong to a series of tetrahedron-shaped clusters termed capped tetrahedral clusters denoted as C*n*.[5] The C*n* series is one of three series of tetrahedral clusters commonly observed in open-framework chalcogenides. Two other series are known as supertetrahedral clusters (T*n*) and penta-supertetrahedral clusters (P*n*). Because of geometric relationships among these clusters, the general stoichiometry of P*n* and C*n* clusters can be derived from the stoichiometry of T*n* clusters (Table 2).[5,16]

The first member (denoted C1) in the C*n* series contains 17 metal sites (e.g., $[Cd_{17}S_4(SPh)_{28}]^{2-}$) while the second member (denoted C2) contains 32 metal sites (e.g., $Cd_{32}S_{14}(SPh)_{36}$·4DMF).[3,9] Note that the anionic sites at four corners can sometimes be partially (for Cd-8 or Cd-17 clusters) or completely occupied with neutral ligands (e.g., $Cd_{32}S_{14}(SPh)_{36}$·4DMF),[9] which serves to reduce the negative charge per cluster.

While the core of a C*n* is a regular fragment of the cubic zinc blende type phase, its four corners are barrelanoid cages possessing the characteristics of the hexagonal wurtzite type phase. For C*n* clusters, each barrelanoid cage $[Cd_4(SPh)_3S]$ at one of four corners can be independently rotated (around the threefold axis of the tetrahedron) by 60°, which results in four additional series of tetrahedral clusters denoted as C*n*,*m* clusters (for n = 1, however, only one corner can be rotated). The integer m refers to the number of corners that have been rotated from their original position in parent C*n* clusters. While C*n* clusters are well-known, examples of C*n*,*m* clusters were rare prior to our work.

Two-dimensional structures reported here consist of Cd-32 clusters with one barrelanoid cage rotated, and such clusters are thus denoted as C2,1 (Figure 1A). In addition, core−shell-like Cd-17 clusters (C1, Figure 1B) have also been synthesized as building blocks in a dimeric assembly.

Factors Affecting Co-Assembly between Chalcogenide Clusters and Bifunctional Ligands. A key factor that controls the connectivity and assembly of chalcogenide clusters is the charge on each precursor cluster and the charge on each ligand. In this work, the charge per cluster is determined by the size of the cluster, and the charge of the ligands is chosen to be neutral. In a simple composition in which the cluster is only terminated with negative −SPh groups (e.g., $Cd_{17}S_4(SPh)_{28}^{2-}$, $Cd_{32}S_{14}(SPh)_{40}^{4-}$), the charges on Cd-17 and Cd-32 clusters are −2 and −4, respectively (Table 2). In principle, up to four terminal −SPh groups can be replaced with neutral bridging ligands; however, the consideration of charge poses a limitation on the number of terminal −SPh groups that can be substituted. Because under solvothermal conditions the formation of positive clusters

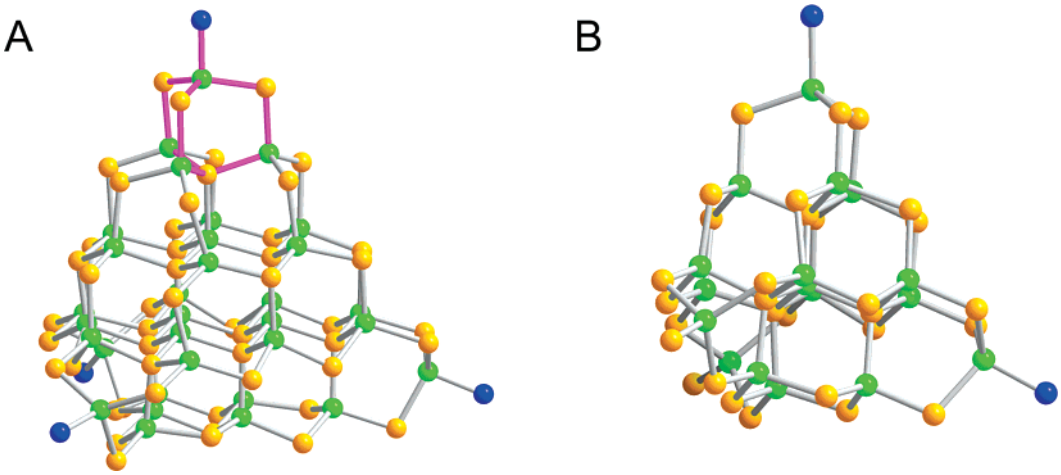

Figure 1. Two different tetrahedral clusters synthesized in this study. (A) The C2,1 cluster in COV-5, and COV-7 has one corner barrelanoid cage rotated. (B) The C1 cluster in COV-8. Green sphere, Cd^{2+}; orange sphere, S/Se; blue sphere, nitrogen in the pyridyl group. Carbons in −SPh and bridging bipyridines are omitted for clarification.

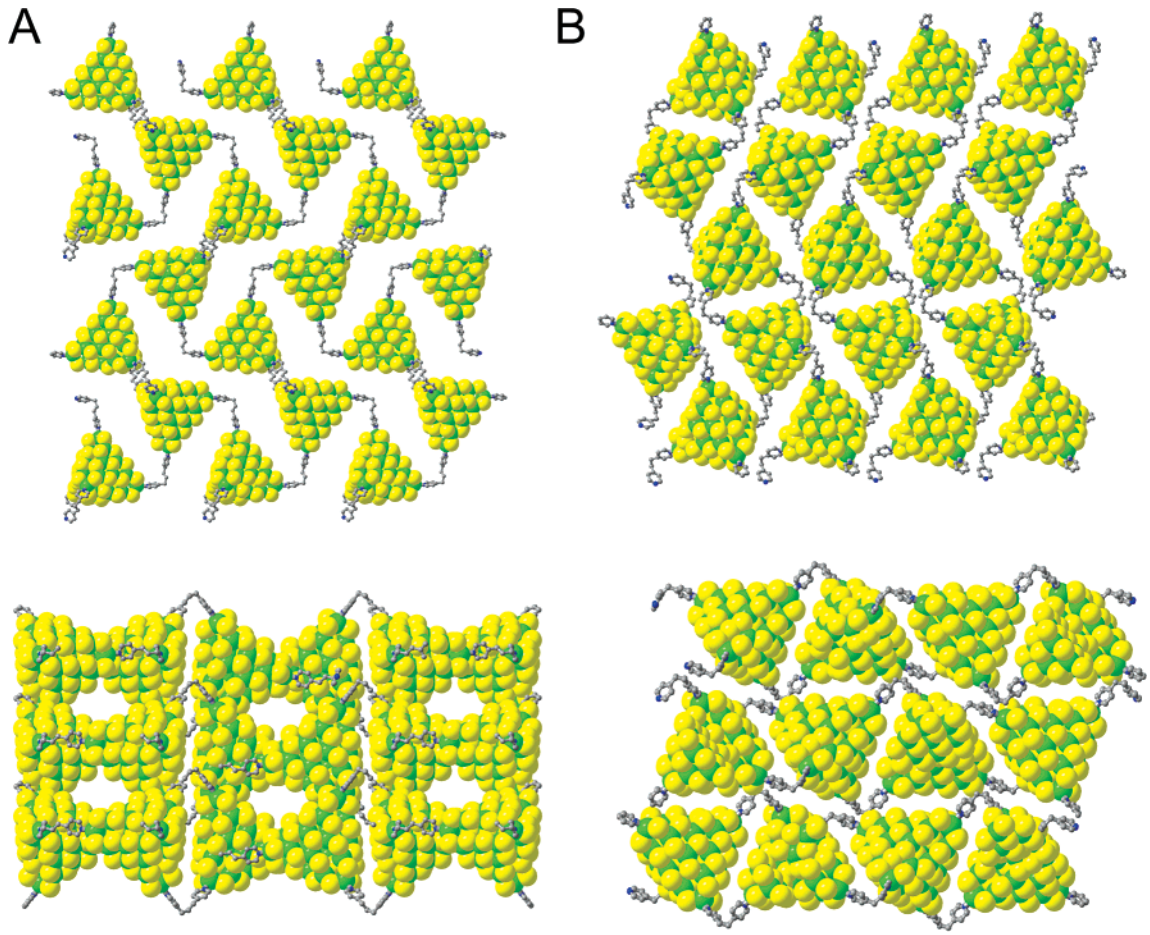

Figure 2. Two-dimensional organization of Cd-32 clusters. (A) In COV-5, C2,1 CdS clusters are connected by 4,4′-trimethylenedipyridine. (B) In COV-7, C2,1 CdS clusters are joined by 1,2-bis(4-pyridyl)ethane molecules. Figures in the second row show the stacking of layers.

has never been observed and is unlikely to form, only two corners of Cd-17 clusters are available for cross-linking whereas Cd-32 clusters can use up to four corners for cross-linking when neutral ligands are employed.

In addition to charges of clusters and ligands, the number of donor atoms on each ligand is also expected to control the assembly and dimensionality of the resulting structures. This work focuses on the use of bidentate ligands (bipyridines in particular).

Co-Assembly between Chalcogenide Clusters and Bifunctional Ligands. Through temperature control, in combination of the optimization of other synthetic parameters such as solvent and molecular precursors, large Cd-32 clusters (C2,1) have been stabilized under solvothermal conditions and co-assembled into two unique two-dimensional superstructures (Figure 2). The common structural pattern in these two-dimensional co-assemblies is the presence of a dimeric unit formed by connecting two Cd-32 clusters through two ligands. The formation of such dimeric units leaves four "free" corners (for each dimer) for cross-linking with other dimers. Each dimer behaves like a pseudo-tetrahedral unit and is joined to four adjacent dimers through four cross-linking ligands to form two-dimensional arrays. Thus, these two-dimensional patterns result from the combined use of single and double organic bridges between inorganic nanoclusters.

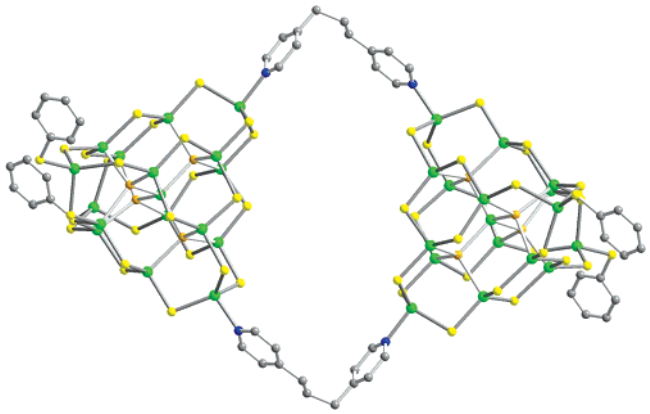

Figure 3. Bridging the gap between discrete clusters and extended covalent assemblies. In COV-8, core−shell-type $Cd_{17}Se_4(SPh)_{26}$ clusters are bridged through two TMDPy molecules into a dimer.

Different bridging ligands can be used for the co-assembly process. In COV-5, TMDPy molecules are used as ligands to bridge C2,1 CdS clusters, whereas in COV-7, C2,1 CdS clusters are jointed through shorter 4,4′-bipyridylethane.

One unique situation is the formation of an isolated dimeric structure. In COV-8, two Cd-17 core−shell-type CdSeS clusters are connected by two TMDPy molecules into an isolated dimer (Figure 3), which subsequently crystallizes into a molecular crystal. Such a dimeric structure illustrates the range of structure types that are accessible through the synthetic method reported here.

Conclusion

The use of bifunctional organic ligands as linkers has been demonstrated as an efficient approach to create zero- and two-dimensional assemblies of chalcogenide tetrahedral nanoclusters. Materials reported here represent just a few examples among many possible superlattices that are accessible through the synthetic approach reported here. This approach holds great promise for the synthetic design of a variety of novel nanocluster superlattices in which the structures and compositions of both nanoclusters and molecular ligands can be tuned to optimize desirable properties. The synergetic effect resulting from the molecular-level integration of optically and electrooptically active inorganic and organic components could lead to new applications that are not accessible with individual nanostructures or their noncovalent assemblies. The remaining challenges include the use of negatively charged, multidentate, or electronically and optically active ligands to create three-dimensional organic−inorganic nanocluster superlattices.

Acknowledgment. The authors acknowledge the support of this work by NSF (P. F.), Beckman Foundation (P. F.), NIH (X. B., Grant: 2 S06 GM063119-05), and ACS-PRF (X. B.). P.F. is a Camille Dreyfus Teacher-Scholar.

Supporting Information Available: Crystallographic data including positional parameters, thermal parameters, and bond distances and angles (CIF). This material is available free of charge via the Internet at http://pubs.acs.org.

CM060557Z